Terra Nova

Shallow necking depth and differential denudation linked to post-rift continental reactivation: the origin of the Cenozoic basins in southeastern Brazil

Journal:	*Terra Nova*
Manuscript ID	TER-2018-0109
Wiley - Manuscript type:	Paper
Date Submitted by the Author:	01-Nov-2018
Complete List of Authors:	Monteiro da Silva, Rafael; Universidade de Sao Paulo Instituto de Astronomia Geofisica e Ciencias Atmosfericas, Geofísica Sacek, Victor; Universidade de Sao Paulo Instituto de Astronomia Geofisica e Ciencias Atmosfericas, Geofísica
Keywords:	southeastern Brazil, lithospheric stress, necking depth, differential denudation, numerical model

Shallow necking depth and differential denudation linked to post-rift continental reactivation: the origin of the Cenozoic basins in southeastern Brazil

Rafael M. Silva[1*], Victor Sacek[1]

[1]Universidade de São Paulo, Instituto de Astronomia, Geofísica e Ciências Atmosféricas, Departamento de Geofísica, Brazil

*Corresponding author:

Rafael M. Silva

E-mail: rmslobato@gmail.com

Phone: +55 11 30914755

Fax: +55 11 30915034

University: Universidade de São Paulo, Instituto de Astronomia, Geofísica e Ciências Atmosféricas

Address: Rua do Matão, 1226, Cidade Universitária, São Paulo-SP, Brasil, 05508-090

Abstract

The southeastern Brazilian margin presents renewed Cenozoic tectonism that created a series of grabens and small sedimentary basins, known as the Continental Rift of Southeastern Brazil. The formation of this rift occurred long after the South Atlantic ocean opening and was attributed to different mechanisms like regional uplift induced by hotspot activity, pulses of Andean orogeny, and reactivation of pre-existing faults. However, the proposed models lack an analytical or numerical verification from a geodynamic point of view. Based on finite element modeling of the lithospheric stress field evolution we conclude that a shallow necking depth, consistent with the hyperextended southeastern Brazilian margin, combined with differential denudation of the continent, results in an upper crustal stress field favorable to normal faulting at the time span of the Cenozoic tectonism.

Keywords: southeastern Brazil, lithospheric stress, necking depth, differential denudation, numerical model

1 Introduction

The Continental Rift of Southeastern Brazil (CRSB) is characterized by several Cenozoic sedimentary basins (Fig. 1A) along a narrow valley flanked by the Serra do Mar and the Serra da Mantiqueira escarpments (Riccomini et al., 2004). The rift extends for about 900 km along the continental margin and follows the direction of dextral strike-slip shear zones (NE-trending) of Precambrian rocks of the Ribeira belt (*e.g.,* Trouw et al., 2000). The formation of the CRSB during the Palaeocene (*e.g.,* Cobbold et al., 2001; Sant'Anna et al., 2004) cannot be explained as a natural consequence of the South Atlantic opening during the Early Cretaceous, with a time interval of more than 60 million years (Myr) between these two events. Different mechanisms were invoked to explain the CRSB formation, like normal fault reactivation of weak Precambrian shear zones, which led to gravitational sliding between the continent and the adjacent offshore basins (*e.g.,* Almeida, 1976; Riccomini et al., 2004), far-field stresses related to Andean orogeny and consequent reactivation of the pre-existing shear zones in a transtensional context (*e.g.,* Cobbold et al., 2001; Cogné et al., 2013), and regional uplift of the margin related to the passage of the Trindade-Martin Vaz hotspot under the continental margin, which resulted in alkaline intrusions (Cobbold et al., 2001) (Fig. 1A).

In spite of the various proposed mechanisms to explain the CRSB generation, there is a lack of quantitative studies to analyze their viability. Using a finite element model to simulate the stress field evolution during the post-rift phase, we conclude that a shallow necking depth (Braun and Beaumont, 1987) during the Cretaceous opening of the South Atlantic ocean combined with differential onshore denudation and offshore sedimentation created a state of stress in the upper crust favorable to normal faulting near the margin at the timing of CRSB formation. Deeper necking depth delays the timing in which normal faulting occurs, whereas regional uplift and horizontal compressive stresses represented secondary factors in the Cenozoic tectonism.

2 Modeling description

Here we used a mechanical, two-dimensional finite element model (Assumpção and Sacek, 2013) in which the rheology of the lithosphere is described by a Maxwell viscoelastic material with a nonlinear power-law viscosity (Melosh and Raefsky, 1980) in plane-strain deformation. The effective viscosity η_{eff} is a function of pressure P and absolute temperature T:

$$\eta_{\text{eff}} = \exp\left(\frac{E_a + PV_a}{RT}\right) / 2A\sigma_{\text{II}}^{n-1} \tag{1}$$

where σ_{II} is the square root of the second invariant of the deviatoric stress tensor and the other parameters are defined in Table 1. The model domain is 2000-km-long by a 150-km-thick lithosphere (L_z). In the continental side of the model, the crust is 40-km-thick, while for the oceanic domain, we assumed a stretching factor β (McKenzie, 1978) of 3, which is representative for the distal southeastern Brazilian margin (Chang et al., 1992). Between the continental and oceanic domains, the crustal thickness varies linearly in a transition zone 60-km-long near the center of the model (Fig. 2). For the reference model, in the onset of the simulation, the lithosphere is in isostatic equilibrium assuming the densities of 2800, 3250 and 3300 kg/m^3 for crust, lithospheric mantle and asthenosphere, respectively. The temperature profile, necessary to calculate the effective viscosity in the crust and mantle, varies linearly from 0 °C at the surface to 1300 °C at the base of the lithosphere in the continental part. In the oceanic part, the profile varies linearly from 0 °C at the bottom of the water layer to 1300 °C at depth L_z/β (thinned lithosphere) and is constant below this depth. The upper and bottom boundaries were left free while the lateral boundaries were kept fixed in the horizontal direction. Winkler's foundation was used to keep isostatic equilibrium.

We performed numerical experiments varying the necking depth of the lithosphere, the denudation and sedimentation rates, the effect of a regional uplift and compressional stresses in the model. In the numerical scenarios, the total amount of erosion in the continent since the opening of the Atlantic margin was 3 km over 100 km near the coastal area, and 1 km in the hinterland, decreasing smoothly to zero landward, and the maximum offshore sedimentation was 4 km (Fig. 2, vertical arrows in the upper panel). This denudation/sedimentation pattern corresponds to setup a and half of these amplitudes represents setup b. For simplicity, we simulated denudation/sedimentation with a constant rate (Fig. 1C, black line). The total simulated time was 130 Myr, equivalent to the age of SE Brazilian margin. The erosion and sedimentation was incorporated in the numerical model as nodal forces at the top of the finite element mesh (Braun and Beaumont, 1987).

Additionally, we tested the effect of a regional uplift that would be caused by a thermal anomaly under the base of the continental lithosphere moving toward the right side of the model, simulating the relative movement of the South American plate over the Trindade-Martin Vaz hotspot. To simulate the uplift, we applied a vertical stress at the bottom nodes of the model resulting in a vertical displacement s:

$$s(x,t) = S \exp\left(-(x - vt - x_0)^2/r^2\right) \tag{2}$$

where S is the maximum amplitude, r is the swell radius, v is the horizontal velocity, t is the time, and x_0 is the initial position of the swell center. We used $S = 1000$ m and $r = 600$ km, corresponding to the approximate dimensions of the present Trindade-Martin Vaz hotspot swell in the Atlantic ocean (Ito and van Keken, 2007) and $v = 2.3$ cm/yr based on Ferrari and Riccomini (1999).

To simulate the flexural effect of different necking depths (z_n) in the model, we applied a vertical load q in the offshore domain given by (Braun et al., 2013)

$$q = (1 - \frac{1}{\beta})[h_{c0}(\rho_m - \rho_c) - (\rho_m - \rho_w)z_n]g \tag{3}$$

where h_{c0} is the original crustal thickness, ρ_m, ρ_c and ρ_w are the mantle, crust and water densities, respectively, and g is the gravitational acceleration. To mimic this q load, we applied a fictitious density contrast $\Delta\rho'$ (Fig. 2) in the thinned crust relatively to the reference model given by

$$\Delta\rho' = \frac{\beta q}{h_{c0} g} \ . \tag{4}$$

To simulate the ridge push force, a horizontal force were applied in the model

$$F(t) = F_{\mathrm{RP}}\left(1 - \exp\left(-t/\tau_{\mathrm{RP}}\right)\right) \tag{5}$$

where τ_{RP} is a decaying control factor and F_{RP} is the maximum force per unit length (see Supporting Information).

To evaluate the brittle failure of rocks we used the Mohr-Coulomb criterion (Ranalli, 1987)

$$\tau = c + \mu\sigma_n \tag{6}$$

where τ is the shear stress, $\mu = \tan\phi$ is the coefficient of friction for the internal friction angle ϕ, σ_n is the normal stress, and c is the cohesion. The depth in which this condition is satisfied we defined as the maximum depth of brittle failure ($d_{\max}$). Our viscoelastic model does not incorporate the brittle deformation mechanism in the constitutive equations and, therefore, cannot simulate faulting. However, $d_{\max}$ gives an estimate of the depth where the brittle limit is achieved for different cohesion values, assuming the stress field in the viscoelastic model for each time step of the simulation.

We performed numerical experiments with different boundary conditions to simulate the effect of surface loads due to denudation and sedimentation (S), regional uplift (U) and horizontal compressive stresses (C), resulting in models labeled S, SU and SC, where more than one letter means combination of effects.

3 Results

In the model S for $z_n = 8.1$ km, in which the lithosphere is initially close to isostatic equilibrium (Fig. 3A, reference model), the unloading caused by concentrated denudation resulted in large tensional horizontal deviatoric stresses in the upper continental crust. These stresses are amplified by the load in the offshore basin. The $d_{\max}$ increases with time near the margin and is deeper for low cohesion values (Fig. 3A). For deeper necking depth ($z_n = 12.1$ km, Fig. 3B), $d_{\max}$ is shallower due to additional compressive stresses in the upper crust originated by upward flexure of the margin.

For different models, Fig. 4 presents the timing t_f when the $d_{\max}$ is deeper than a threshold depth, assumed here equal to 1 km bellow the eroded surface. The timing in which t_f occurs increases for deeper necking depths, varying more than 10 Myr for a 1 km change in z_n. Additionally, the decrease in amplitude of the surface processes (models b) delayed the t_f by up to ∼60 Myr.

Regional uplift (models SU) changed t_f by less than 10 Myr in almost all the models, representing a secondary tectonic effect. In fact, the regional uplift did not significantly modified the deviatoric stress pattern in the upper crust. Regional compression (models SC) tends to delay the t_f, but this effect is significant only for models with low denudation rate (models b). Therefore, the main factors that controls the timing of t_f are the necking depth and the magnitude of the surface processes.

4 Discussion

The hyperextended SE Brazilian margin is marked by a wide continent-ocean transition with more than 500 km, which is compatible with a shallow necking depth (Huismans and Beaumont, 2011), probably <12 km. This shallow necking depth combined with the high denudation concentrated along the margin predicted by themochronological data, reaching up to 4 km of post break-up denudation (Cogné et al., 2011), can explain the origin of the CRSB during the Paleocene.

As our model does not incorporate the brittle rheology, the present viscoelastic model cannot simulate faulting in upper part of the continental crust during the margin evolution. However, the $d_{\max}$ gives the depth of the envelope where the brittle limit is achieved for different cohesion values, assuming the stress field in the viscoelastic model for each time step of the simulation. Incorporation of brittle rheology would modify the stress field mainly in the upper crust, localizing the deformation and, eventually, resulting in deeper faults. In fact, previous thermomechanical models with a nonlinear brittle-elastic-ductile rheology showed that erosion indeed induces localization, increasing the deformation rate along major faults (*e.g.,* Burov and Poliakov, 2001).

Although we employed a very simplified erosion history assuming a constant rate of erosion with total denudation up to 3 km, representing a lower boundary for the total denudation in southeastern Brazil since the Early Cretaceous, thermochronological data (*e.g.*, Cogné et al., 2011) indicates that denudation rate changed through time, with high cooling rates between 90 and 60 Ma (Fig. 1C). These simulations show that considering a high denudation rate of the continental margin combined with sedimentary deposition in the oceanic domain leads to an expressive contribution to the normal faulting reactivation of the Precambrian shear zones of the Ribeira belt where the rocks of upper crust had lower internal cohesion. Additionally, our results indicate that other geotectonic processes like regional uplift and compression had secondary effect on the formation of these normal faults. However, a regional uplift can be indirectly related to the rift formation by the perturbation of surface processes dynamics, contributing to enhance denudation. Braun et al. (2013b) showed that long-wavelength topographic perturbation due to a mantle source can induce high denudation even for a broad and smooth uplift. Thus, in spite of the inexpressive modification of the deviatoric stresses in the upper crust due to regional uplift, this perturbation probably increased the denudation rate in the onshore margin.

We conclude that important elements to create the CRSB are: (i) a shallow necking depth, (ii) the high denudation concentrated along the continental margin, and (iii) the preexistence of shear zones parallel to the coast. Other divergent margins around the world probably do not present these factors simultaneously, hence not inducing the formation of a continental rift. Thermochronological data (O'Sullivan et al., 1996) indicate that the divergent margin of southeastern Australia, formed at 100-90 Ma, had a low post-rift denudation rate, which might have contributed to the inexpressive post-breakup tectonism of this margin (*e.g.*, Bishop and Goldrick, 2000). In the margin between Namibia and South Africa the denudation was about the same magnitude observed in SE Brazil (Gallagher and Brown, 1999). However, in this case, the width of the mobile belt parallel to coast is much narrower than the Ribeira Belt, hence not favoring the formation of a fault system on the belt. For non-hyperextended margins, necking depth is expected to be higher, inducing upward flexure of the margin and precluding normal faulting occurrence. The Araçuaí Belt, northward of the Ribeira Belt, and the West Congo Belt in the African conjugate margin evolved to relatively narrow margins and, therefore, probably related to deeper necking depths, which in turn contributed to suppress post-rift normal faulting reactivations.

5 Conclusions

This study provides a numerical quantification of the stresses within the lithosphere due to variable necking depth, onshore erosion, offshore sedimentation, regional uplift and compressional stresses based on numerical simulation of the southeastern Brazilian margin evolution using a viscoelastic numerical model. Our results showed a dependence between the necking depth of the lithosphere and the timing in which normal faulting is expected to occur in the upper crust near the margin. A shallow necking depth (≤ 12 km) together with the high denudation rate of the onshore area, which resulted in more than 3 km of erosion along the margin since the opening of South Atlantic ocean, combined with the pre-existing shear zones parallel to the margin contributed to form a suitable scenario for the formation of the Continental Rift of southeastern Brazil. On the other hand, a regional uplift induced by the relative movement of the South American plate over the Trindade-Martin Vaz hotspot cannot explain the reactivation of deep normal faults by flexural stresses.

6 Acknowledgments

This work was supported by PRH-ANP and FAPESP 2017/10554-4 scholarships to R.M.S. and grants FAPESP 2017/24870-5 and CNPq 311315/2017-8 to V.S. This study was financed in part by the Coordenação de Aperfeiçoamento de Pessoal de Nível Superior - Brasil (CAPES) - Finance Code 001. This project used computational resources obtained from Petrobras (contract number 4600365494).

References

Almeida, F.F.M.D., 1976. The system of continental rifts bordering the Santos Basin, Brazil, *Anais da Academia Brasileira de Ciências*, **48**, 15–26.

Assumpção, M. and Sacek, V., 2013. Intra-plate seismicity and flexural stresses in central Brazil, *Geophysical Research Letters*, **40**(3), 487–491.

Bishop, P. and Goldrick, G., 2000. Geomorphological evolution of the East Australian continental margin. In: *Geomorphology and Global Tectonics* (M.A. Summerfield, ed). Wiley, Chichester, UK, pp. 227–255.

Braun, J. and Beaumont, C., 1987. Styles of continental rifting: Results from dynamic models of lithospheric extension. In: *Sedimentary Basins and Basin-Forming Mechanisms* (C. Beaumont and A.J. Tankard, eds). *Mem. Can. Soc. Pet. Geol.*, **12**, 241–258.

Braun, J., Deschamps, F., Rouby, D. and Dauteuil, O., 2013. Flexure of the lithosphere and the geodynamical evolution of non-cylindrical rifted passive margins: Results from a numerical model incorporating variable elastic thickness, surface processes and 3D thermal subsidence, *Tectonophysics*, **604**, 72–82.

Braun, J., Robert, X. and Simon-Labric, T., 2013b. Eroding dynamic topography, *Geophysical Research Letters*, **40**(8), 1494–1499.

Burov, E. and Poliakov, A., 2001. Erosion and rheology controls on synrift and postrift evolution: Verifying old and new ideas using a fully coupled numerical model, *Journal of Geophysical Research, Solid Earth*, **106**(B8), 16461–16481.

Chang, H.K., Kowsmann, R.O., Figueiredo, A.M.F. and Bender, A., 1992. Tectonics and stratigraphy of the East Brazil Rift system: an overview, *Tectonophysics*, **213**(1), 97–138.

Cobbold, P.R., Meisling, K.E. and Mount, V.S., 2001. Reactivation of an obliquely rifted margin, Campos and Santos basins, southeastern Brazil, *AAPG Bulletin*, **85**(11), 1925–1944.

Cogné, N., Cobbold, P.R., Riccomini, C. and Gallagher, K., 2013. Tectonic setting of the Taubaté Basin (southeastern Brazil), Insights from regional seismic profiles and outcrop data, *Journal of South American Earth Sciences*, **42**, 194–204.

Cogné, N., Gallagher, K. and Cobbold, P.R., 2011. Post-rift reactivation of the onshore margin of southeast Brazil: evidence from apatite (U–Th)/He and fission-track data, *Earth and Planetary Science Letters*, **309**(1-2), 118–130.

Contreras, J., Zühlke, R., Bowman, S. and Bechstädt, T., 2010. Seismic stratigraphy and subsidence analysis of the southern Brazilian margin (Campos, Santos and Pelotas basins), *Marine and Petroleum Geology*, **27**(9), 1952–1980.

Ferrari, A.L. and Riccomini, C., 1999. Campo de esforços plio-pleistocênicos na Ilha da Trindade (Oceano Atlântico Sul, Brasil) e sua relação com a tectônica regional, *Rev. Bras. Geociênc.*, **29**(2), 195–202.

Gallagher, K. and Brown, R., 1999. The Mesozoic denudation history of the Atlantic margins of southern Africa and southeast Brazil and the relationship to offshore sedimentation, *Geological Society, London, Special Publications*, **153**(1), 41–53.

Huismans, R. and Beaumont, C., 2011. Depth-dependent extension, two-stage breakup and cratonic underplating at rifted margins, *Nature*, **473**(7345), 74.

Ito, G. and van Keken, P.E., 2007. Hotspots and melting anomalies. In: *Treatise on Geophysics: Mantle Dynamics, Vol. 7* (D. Bercovici, ed). Elsevier.

Karato, S.I. and Wu, P., 1993. Rheology of the upper mantle, A synthesis, *Science*, **260**(5109), 771–778.

McKenzie, D., 1978. Some remarks on the development of sedimentary basins, *Earth and Planetary Science Letters*, **40**(1), 25–32.

Melosh, H.J. and Raefsky, A., 1980. The dynamical origin of subduction zone topography, *Geophysical Journal International*, **60**(3), 333–354.

O'Sullivan, P.B., Foster, D.A., Kohn, B.P. and Gleadow, A.J., 1996. Multiple postorogenic denudation events: An example from the eastern Lachlan fold belt, Australia, *Geology*, **24**(6), 563–566.

Ranalli, G., 1987. *Rheology of the Earth, Deformation and Flow Processes in Geophysics and Geodynamics*. Allen and Unwin, Boston, 366 pp.

Riccomini, C., Sant'Anna, L. and Ferrari, A., 2004. Evolução geológica do rift continental do sudeste do Brasil. In: *Geologia do continente Sul-Americano: evolução da obra de Fernando Flávio Marques de Almeida* (V. Mantesso-Neto, A. Bartorelli, C.D.R. Carneiro and B.B.B Neves, eds). Beca, São Paulo, pp. 383–405.

Sant'Anna, L., Riccomini, C., Rodrigues-Francisco, B., Sial, A., Carvalho, M. and Moura, C., 2004. The Paleocene travertine system of the Itaboraí basin, Southeastern Brazil, *Journal of South American Earth Sciences*, **18**(1), 11–25.

Trouw, R.A.J., Heilbron, M., Ribeiro, A., Paciullo, F., Valeriano, C.M., Almeida, J.C.H., Tupinamba, M. and Andreis, R.R., 2000. The central segment of the Ribeira Belt. In: *Tectonic Evolution of South America* (U.G. Cordani, E.J. Milani, A. Thomas Filho, D.A. Campos, eds). Fundo Setorial de Pet. e Gás Nat., Rio de Janeiro, pp. 287–310.

Figure captions

Figure 1. A: Map of southeastern Brazil. Black arrows indicate the Serra da Mantiqueira and the Serra do Mar escarpments. Triangles are locations of thermochronological data (Cogné et al., 2011). Lower inset shows the geologic context of the CRSB. Orange areas are the CRSB basins and solid traces are main Precambrian shear zones (redrawn from Cogné et al. (2011)). **B:** Elevation profile showed in A as XX'. Sedimentary stratigraphic profile YY' in A was obtained from (Contreras et al., 2010). Upper panel are the maximum post-rift denudation inferred from the thermochronological data considering a geothermal gradient of 30 °C/km. **C:** Representative denudation and sedimentation evolution patterns used in the model (black curve). The maximum magnitude varied across the model as shown in Fig. 2 (upper panel). The colored curves represent the thermal histories obtained from Cogné et al. (2011) with the respective colors of total denudation shown in B.

Figure 2. Model setup. Density contrasts were calculated based on reference densities for the crust and mantle of 2800 and 3250 kg/m^3, respectively. The dashed rectangle indicates the sections shown in Fig. 3. The swell profile in the bottom part represents a thermal anomaly moving rightward with velocity of 2.3 cm/yr. Arrows in the upper panel represent the maximum load variation across the model. $\Delta\rho'$ is a fictitious density contrast used to obtain the equivalent flexural load for a given necking depth. The denudation/sedimentation rates follows the linear pattern shown in Fig. 1C.

Figure 3. Deviatoric stress pattern along the continental margin for models with only surface processes (models S and setup a). Only a section of the numerical domain is shown (see Fig. 2 for location). Column **A** is for $z_n = 8.1$ km and column **B** for $z_n = 12.1$ km. Blue and red line segments represent principal compression and tension, respectively.

Solid, dashed and dotted black lines are the failure limit assuming rock cohesion of 0, 50 and 100 MPa and with $\mu = \tan 30°$. Top horizontal bar indicates the Serra da Mantiqueira (light green), the CRSB (light brown) and the Serra do Mar (dark green) areas. Dark gray area in the section corresponds to the mantle. See Figs. S2 and S3 in Supporting Information for a detailed evolution of the models.

Figure 4. Timing when $d_{\max}$ is deeper than 1 km bellow the eroded surface for different necking depths. The purple (Ar-Ar ages) and magenta (K-Ar ages) bars represent interbedded lava flows with sediments in CRSB basins (Riccomini et al., 2004, and references therein). Horizontal orange bar indicates the Paleocene epoch. The model keys are: S - denudation and sedimentation; SU - denudation, sedimentation, and regional uplift; SC - denudation, sedimentation, and horizontal compression. Total amount of denudation and sedimentation are, respectively, 3 km and 4 km for a and 1.5 km and 2 km, respectively, for b.

Supplementary information

- Description of the ridge push force to simulate a horizontal compressive stress in the model.
- Figure S1. Accumulated erosion and sedimentation during the simulation.
- Figure S2. Evolution of deviatoric stresses pattern for model S and setup a with necking depth $z_n = 8.1$ km.
- Figure S3. Evolution of deviatoric stresses pattern for model S and setup a with necking depth $z_n = 12.1$ km.

Tables

Table 1: Fixed Parameters

	Crust (Ranalli, 1987)	Mantle (Karato and Wu, 1993)
A ($\mathrm{Pa}^{-n}\mathrm{s}^{-1}$)	2.1×10^{-23}	2.4×10^{-16}
E_a (kJ/mol)	238	540
V_a ($\mathrm{m}^3\mathrm{mol}^{-1}$)	0	2×10^{-5}
n	3.2	3.5
R	$8.314\ \mathrm{J\,K^{-1}mol^{-1}}$	
E (Young's modulus)	70 GPa	
ν (Poisson's ratio)	0.25	
g (gravity)	$9.8\ \mathrm{m/s^2}$	
F_{RP} (maximum force)	$4.93\times10^{12}\ \mathrm{N\ m^{-1}}$	
τ_{RP} (exponential factor)	60 Myr	

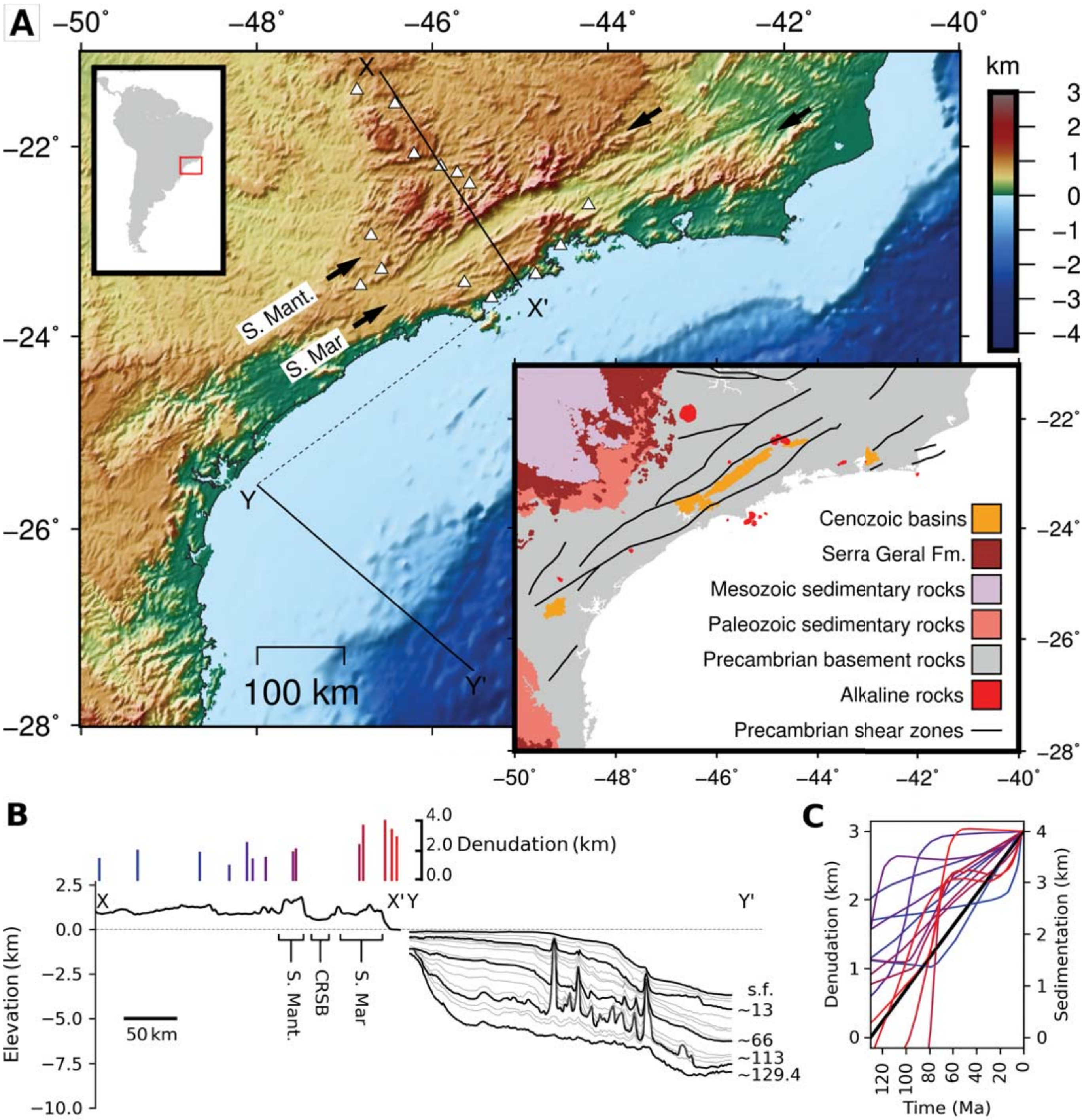
A
−50˚
−48˚
−46˚
−44˚
−42˚
−40˚
−22˚
−24˚
−26˚
−28˚
X
X'
Y
Y'
S. Mant.
S. Mar
100 km
km
3
2
1
0
−1
−2
−3
−4
Cenozoic basins
Serra Geral Fm.
Mesozoic sedimentary rocks
Paleozoic sedimentary rocks
Precambrian basement rocks
Alkaline rocks
Precambrian shear zones
B
4.0
2.0 Denudation (km)
0.0
2.5
0.0
−2.5
−5.0
−7.5
−10.0
Elevation (km)
50 km
S. Mant.
CRSB
S. Mar
s.f.
~13
~66
~113
~129.4
C
Denudation (km)
Sedimentation (km)
Time (Ma)
120
100
80
60
40
20
0

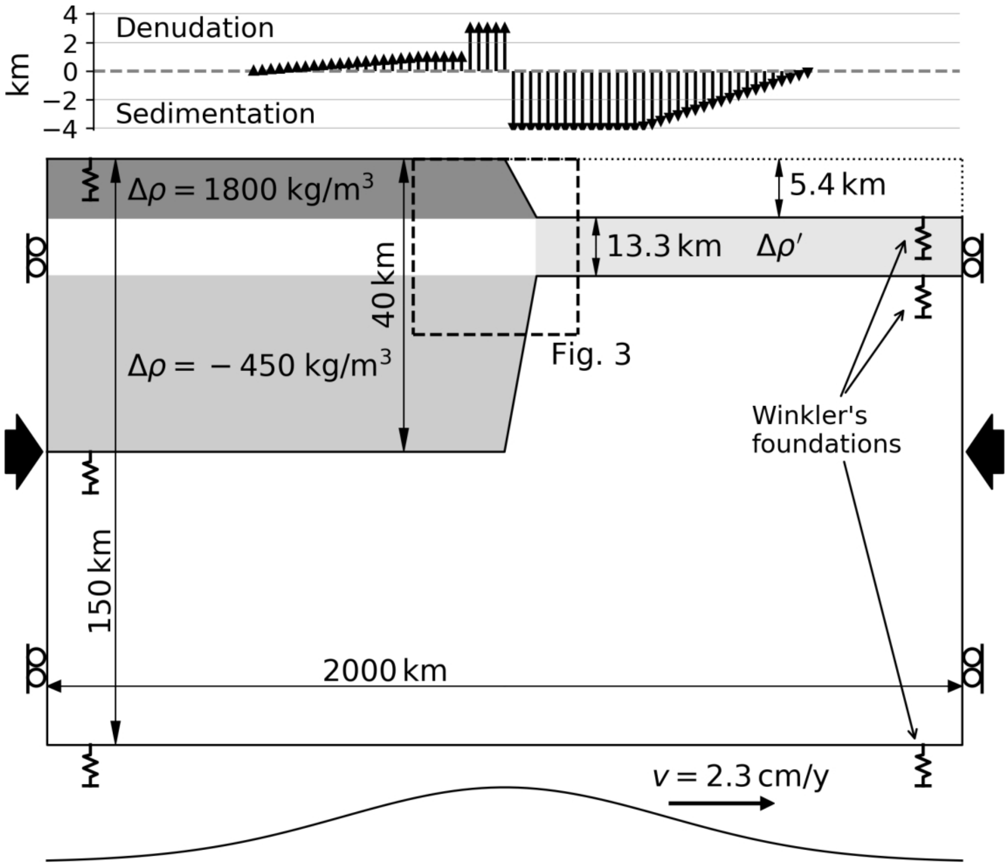

Model setup. Density contrasts were calculated based on reference densities for the crust and mantle of 2800 and 3250 kg/m^3, respectively. The dashed rectangle indicates the sections shown in Fig. 3. The swell profile in the bottom part represents a thermal anomaly moving rightward with velocity of 2.3 cm/yr. Arrows in the upper panel represent the maximum load variation across the model. Δρ' is a fictitious density contrast used to obtain the equivalent flexural load for a given necking depth. The denudation/sedimentation rates follows the linear pattern shown in Fig. 1C.

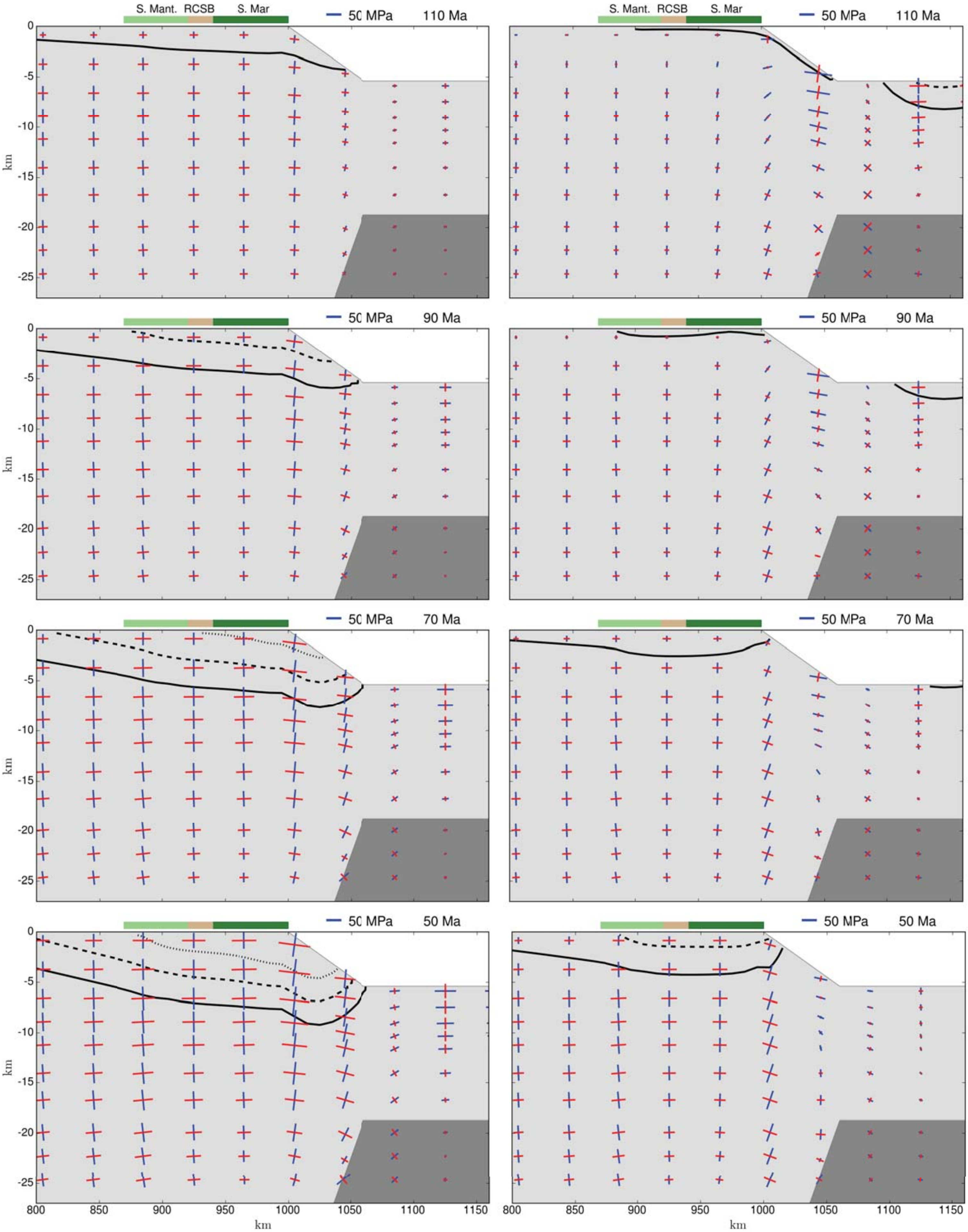
S. Mant.
RCSB
S. Mar
50 MPa
110 Ma
90 Ma
70 Ma
50 Ma
km
0
-5
-10
-15
-20
-25
800
850
900
950
1000
1050
1100
1150
km

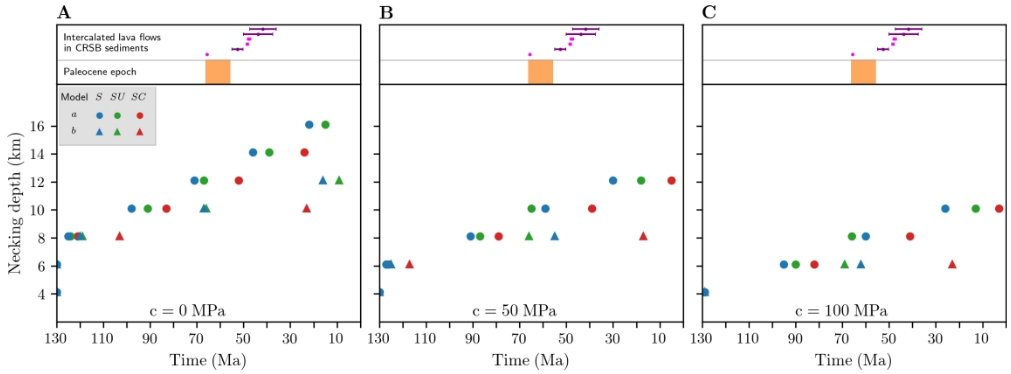

Timing when d_{max} is deeper than 1 km bellow the eroded surface for different necking depths. The purple (Ar-Ar ages) and magenta (K-Ar ages) bars represent interbedded lava flows with sediments in CRSB basins (Riccomini et al., 2004, and references therein). Horizontal orange bar indicates the Paleocene epoch. The model keys are: S - denudation and sedimentation; SU - denudation, sedimentation, and regional uplift; SC - denudation, sedimentation, and horizontal compression. Total amount of denudation and sedimentation are, respectively, 3 km and 4 km for a and 1.5 km and 2 km, respectively, for b.